Photochemical & Photobiological Sciences

RSC Publishing

PAPER

View Article Online
View Journal | View Issue

Cite this: *Photochem. Photobiol. Sci.*, 2013, **12**, 2146

Energy and electron transfer processes in polymeric nanoparticles†

Claudia Solis, Juan J. Torres, Natalia Gsponer, Carlos Previtali, Rodrigo Palacios, Hernán Montejano and Carlos Chesta*

We report herein a study on photoinduced electron transfer (eT) and energy transfer (ET) processes occurring between 9-methylanthracene-acrylate (A) and *N*,*N*-dimethylaniline-acrylate (D) derivatives incorporated into polymeric nanoparticles (NP). Five types of NPs were synthesized: PAD0, PAD25, PAD75, PD25, and PD75. All NPs are composed of a crosslinked polymer matrix of methyl methacrylate and ethylene glycol dimethacrylate. In addition, PAD0, PAD25 and PAD75 contain low doping levels of A. For PAD25 and PAD75, 25% and 75% of the mole fraction of methyl methacrylate is replaced by D, respectively. PD25 and PD75 were prepared as above but without A. NPs (diameter 6–9 nm) dispersed in organic solvents were characterized based on their UV-visible absorption, emission, excitation, and excitation anisotropy spectra and time dependent absorption and emission spectroscopy techniques. The emission decay profiles of A and D were always complex. Results indicate that A senses two distinct environments in all NPs. The emission quenching of PAD0 by DMA in DCM solutions is dynamic, and it is apparent that a significant fraction of A is inaccessible to the quencher. The emission of A is efficiently quenched by the presence of D in PAD25 and PAD75. The intra-NP photoinduced eT quenching mechanism has static and dynamic components. Selective excitation of D in PAD25 and PAD75 leads to the formation of the excited state of A *via* a singlet–singlet ET Föster type mechanism. Results indicate that both intra-NP eT and ET processes are more efficient in PAD75 due to the reduced average D*–A separation in these NPs.

Received 13th June 2013,
Accepted 16th September 2013

DOI: 10.1039/c3pp50183c

www.rsc.org/pps

1. Introduction

Molecular imprinting is a technique that allows the fabrication of polymeric matrices (MIP) with specific molecular recognition binding sites for practically any compound (target) of interest.[1] During the last few decades, this technique was successfully applied to solve a wide range of problems such as chromatography separations,[2,3] drug delivery,[4] molecular sensing,[3] *etc.*

Probably, one of the most appealing applications of MIPs is their potential use as optical sensors. However, a challenge for this particular application is finding an efficient way to transduce the analyte/MIP rebinding event in a measurable signal. Different strategies have been proposed to solve this issue.[5] Among these, the synthesis of MIPs using fluorescent monomers able to be quenched by the analyte *via* photoinduced electron transfer (PeT) or energy transfer (ET) processes is a simple and attractive approach.

However, it is well known that MIPs are highly microheterogeneous materials, usually showing broad distributions of affinity binding sites for the analyte.[6] Hence, quenching of the transducer emission by analyte always results in an intricate kinetics.[7] Interestingly, similarly complex behaviors are also observed in the elementary processes involved in several cutting-edge technologies such as solar cells,[8–12] light emitting diodes,[13–15] field effect transistors,[16–20] optical sensors,[21,22] *etc.* Hence, the study of the dynamics of photoinduced eT and ET processes in microheterogeneous environments[23–28] has become a research topic of significant academic and technological interest.

We report herein a relatively simple study on the PeT and ET processes occurring in polymeric nanoparticles (NP). These studies are part of a more comprehensive project currently under development, which involves the synthesis of MIP nanoparticles and their application as optical sensors. However, before studying the actual MIPs, we considered that it would be useful to investigate simpler systems, namely non-imprinted NP containing well-characterized fluorophores that can emulate the behavior of the transducer (or analyte) in the optical sensor.

For this purpose, anthracene (A) and *N*,*N*-dimethylaniline (D) derivatives (Scheme 1) were incorporated through covalent binding to the matrices of polymeric NP. The NPs synthesized

Departamento de Química, Facultad de Ciencias Exactas, Físico-Químicas y Naturales, Universidad Nacional de Río Cuarto, 5800-Río Cuarto, Argentina. E-mail: cchesta@exa.unrc.edu.ar; Fax: +54 358 4676233; Tel: +54 358 4676523

†Electronic supplementary information (ESI) available. See DOI: 10.1039/c3pp50183c

can be dispersed in organic solvents. The dispersions are optically transparent, stable for months and for many purposes they can be treated as actual solutions.

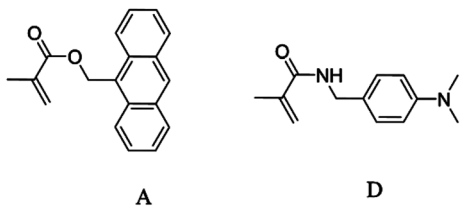

Scheme 1

Five different types of NPs were prepared: PAD0, PD25, PD75, PAD25 and PAD75. The NPs were characterized in DCM and THF suspensions and their photophysical properties were exhaustively studied. PAD0 is a crosslinked copolymer of methyl methacrylate (MMA), ethylene glycol dimethacrylate (EGDMA) and A in a 93 : 53 : 1 molar ratio, respectively. For the synthesis of PAD25 and PAD75, 25% and 75% of the total moles of MMA were replaced by moles of D, respectively, keeping constant the molar ratio of EGDMA and A. PD25 and PD75 were prepared in an analogous manner to PAD25 and PAD75 but they do not contain A.

The manuscript is organized as follows. In section 2, the preparation of the nanoparticles is described. In section 3.1, the characterization of PAD0, PD25 and PD75 using diverse spectroscopic techniques is discussed in detail. In section 3.2, a study on the quenching of the first excited singlet state of A (A*) in PAD0 by *N*,*N*-dimethylaniline in DCM solutions is reported and analyzed. In section 3.3 we present the results of a study of intra-NP photoinduced eT (PeT) processes occurring in PAD25 and PAD75 upon selective excitation of the anthracenyl (A) fluorophore. Finally, by excitation of the D chromophore in PAD25 and PAD75, formation of the singlet excited state of A was observed. A study of these intra-NPs ET processes is reported in section 3.4.

2. Material and methods

2.1 Reagents

Water, dichloromethane (DCM), *c*-hexane, tetrahydrofuran (THF) and acetonitrile, all of HPLC grade, were provided by Sintogran Argentina and used as received. Hexadecyltrimethylammonium bromide (CTAB) (~99%, Sigma-Aldrich Argentina), 1-hexanol (>99%, Fluka), VA-044 (2,2′-azobis[2-(2-imidazolin-2-yl)propane]dihydrochloride) (95%, Wako Pure Chemical Industries), 9-anthracenylmethyl methacrylate (A) (95%, Sigma-Aldrich Argentina), sodium perchlorate monohydrate (>98%, Sigma-Aldrich Argentina), 9-methylanthracene (9MA) (98%, Aldrich). 4-(Dimethylamino)benzylamine dihydrochloride (98%, Aldrich), methacryloyl chloride (97%, Aldrich), and potassium phosphate monobasic (>99.5%, Fluka) were used as received without further purification. Methyl methacrylate (MMA) (~98%, Sigma-Aldrich Argentina) and ethylene glycol dimethacrylate (EGDMA) (98%, Sigma-Aldrich Argentina) were purified prior to polymerization using a chromatographic column filled with De-HiBit-200 (Polysciences, Inc.) which specifically retains monomer stabilizing agents. *N*,*N*-Dimethylaniline (DMA) (99%, Aldrich) was purified by distillation.

2.2 Synthesis

2.2.1 Synthesis of *N*-(4-dimethylamino-benzyl)-2-methyl-acrylamide (D). D was prepared by the reaction of *N*-(4-aminomethyl-phenyl)-dimethyl-amine dihydrochloride and 2-methyl-acryloyl chloride as follows. 40 ml of DCM, 50 ml of a KH_2PO_4/K_2HPO_4 (pH = 7) buffer solution (0.3 M) containing 1 g (4.48×10^{-3} mol) of 4-(dimethylamino)benzylamine dihydrochloride and 10 mg of $NaNO_2$ were mixed by vigorous stirring in a round-bottom flask. The mixture was kept at 0 °C in an ice/water bath. Always under stirring, 380 μl of freshly distilled 2-methylacryloyl chloride dissolved in 4 ml of DCM was added dropwise. After one hour, the organic phase was separated and dried and finally evaporated under reduced pressure. The solid obtained was recrystallized twice from *c*-hexane to yield 0.41 g of *N*-(4-dimethylamino-benzyl)-2-methyl-acrylamide (~43% yield). ^{1}H NMR (CCl_3D): δ 1.96 (m, 3H), 2.94 (m, 6H), 4.38 (m, 2H), 5.31 (m, 1H), 5.65 (m, 1H), 5.97 (m, 1H), 6.69 (m, 2H), 7.18 (m, 2H). ^{13}C NMR ($CDCl_3$): δ 18.3, 40.79, 43.5, 113.1, 119.9, 125.7, 129.1, 140.0, 150.6, 168.0. Mass: (*m*/*z*): 218 [M^+], 201, 174, 148, 134, 118, 91, 77 and 69. IR (KBr): 790, 808, 920, 1226, 1350, 1330, 1525, 1615, 1653 cm^{-1}. UV (DCM) λ^{max} (ε/M^{-1} cm^{-1}): 263 nm (4540), 306 nm (680).

2.2.2 Synthesis of the polymeric NPs. NPs were synthesized by the microemulsion method.[29,30] The procedure for the synthesis of PAD0 is described below. The molar ratio of reactants used for the synthesis of each particle type is shown in Table 1-ESI.†

2.2.2.1 Syntheses of PAD0. Initially, 0.2 g of CTAB (5.5×10^{-4} mol) was dissolved in 100 ml of water. To this solution, 2.6 mg of A (1.12×10^{-4} mol), 100 μl of MMA (9.35×10^{-4} mol) or the corresponding mol of D and 110 μl of EGDMA (5.3×10^{-4} mol) were added. The vinyl polymerization was thermally initiated using 20 mg of VA-044. Oxygen was displaced from the aqueous solution by bubbling N_2 for about 20 min. The synthesis was carried out in a specially designed reactor that avoids the loss of material due to foaming during oxygen purging. The reactor was submerged in a water bath at 40 °C and the mixture was left to react for 24 hours. The micellar solution was transparent both before and after polymerization. The nanoparticles were recovered from micellar medium as follows. The surfactant and particles were precipitated by the addition of 0.1 g of $NaClO_4$ dissolved in 2 ml of water. The solid obtained (a mixture of $CTAClO_4$ and NPs) was filtered-out, and dried under reduced pressure. Fig. 1-ESI† shows the FT-IR of PAD0 and $CTAClO_4$, both physically dispersed in KBr. Finally, the solid was partially resuspended by sonication in 20 ml of an acetonitrile–water mixture (50 : 50 by volume). $CTAClO_4$ is fully soluble in this medium, while the NPs are not. The particles were recovered by ultracentrifugation (30 min, 13 000 rpm). This procedure was repeated several

times until the disappearance of the band at 617 cm^{-1} in the IR spectrum corresponding to perchlorate salt.

Relatively large masses of the NPs can be readily dispersed in solvents such as dichloromethane or chloroform to achieve concentrations up to 5 mg ml^{-1}. Dilute stable dispersions can also be prepared in acetonitrile, THF, ethyl acetate, *etc.* The dispersions are fully transparent and stable for months and can be treated as true solutions for most purposes. All the NPs studied were spectrally stable under the irradiation conditions used for the steady state absorption and emission and transient emission spectroscopic studies. However, slight photobleaching of the anthracene chromophore (and the development of an intense yellow color in the case of PAD25 and PAD75) was observed when the dispersions were illuminated with high intensity pulsed sources (*i.e.* laser flash experiments).

The average hydrodynamic diameter for each particle type was estimated by dynamic light scattering (DLS). Results are presented in Table 2-ESI.†

2.4 Instrumental

UV-Vis absorption spectra were obtained using a Shimadzu UV-2401 spectrophotometer. FT-IR spectra were recorded using a Nicolet Impact 400. Proton nuclear magnetic resonance spectra were recorded using an FT-NMR Bruker Advance 200 spectrometer at 200 MHz. Mass spectra were taken with a CG Hewlett Packard 5890 coupled to a series 5972 mass selective detector.

DLS measurements were obtained using a Malvern 4700 instrument (with a goniometer and a 7132 correlator) with an argon-ion laser operating at 488 nm; all experiments were carried out at 90° scattering angle at 298 K. NP suspensions were filtered through 200 nm pore filters right before data acquisition. Extreme care was taken to reduce the contamination by dust.

Steady-state fluorescence measurements were performed using a Fluoromax Spex spectrofluorometer. Freshly prepared nanoparticle dispersions were used for each measurement and the absorbance was adjusted to <0.05 at the excitation wavelength. Fluorescence quantum yields ϕ_f for the anthracenyl fluorophore (A) in PAD0, PAD25 and PAD75 were determined relative to that of 9-methylanthracene (9-MA) in *c*-hexane (ϕ_f = 0.35).[31] Similarly, approximate values of ϕ_f for the emission of D in PD25, PD75, PAD25 and PAD75 were measured relative to that of DMA in *c*-hexane (ϕ_f = 0.11).[31] In both cases, suitable corrections for the refractive index of the solvents were performed.[32]

Fluorescence-lifetime measurements were performed using an Edinburgh Instruments (TC-SPC 900) time-correlated single-photon counting fluorometer. The excitation of the samples was carried-out using PicoQuant PLS297 or PL378 diodes depending upon the experiment. Fluorescence decays were fitted to mono- or multiexponential decay functions. The criteria used to judge the goodness of the fits were χ^2 and the weighted residuals (*Ri*). The parameters obtained from the fitting of the experimental decay curves were taken as acceptable when the calculated χ^2 was found to be in the range: 0.85 < χ^2 < 1.15. In the case of multiexponential decays, the mean lifetimes were calculated according to:[32,33]

$$\tau_M = \frac{\sum_i a_i \tau_i}{\sum_i a_i} \quad (1)$$

where a_i and τ_i are the corresponding amplitudes and lifetimes of the *i*th component of the multiexponential decay.

Emission decays were also interpreted using the lifetime's distribution analysis software provided by Edinburgh Instruments (*i.e.* the EI method). Details of the algorithm used by the EI method to find the lifetime's distribution that best fits the experimental decays has been discussed elsewhere.[7,34–37] The EI method assumes that the theoretical decay function, $I(t)$, is given by:

$$I(t) = \int_0^\infty \alpha(\tau) \exp(-t/\tau) d\tau \quad (2)$$

where $\alpha(\tau)$ is a continuous distribution of lifetimes. In principle, the method finds the $\alpha(\tau)$ that best fits the experimental decay profile. To this end, the temporal scale is divided into a finite number (n) of logarithmically equally spaced lifetimes. Within this approximation, $I(t)$ can be written as a multiexponential decay function according to:

$$I(t) = \sum_{i=1}^{n} \alpha_i \exp(-t/\tau_i) \quad (3)$$

In this study, all EI lifetime's distributions were obtained using 50 lifetimes (n = 50, eqn (3)). The minimum τ_i was set always as 100 ps (*i.e.* the best temporal resolution of our instrument). The maximum τ_i was varied depending upon the emission properties of the fluorophore studied. As a rule, τ_i^{max} was set as 4 times the longer lifetime obtained from the standard multiexponential analysis of the samples. The lifetime's distributions are histograms representing the normalized amplitudes (α_i/α_i^{max}) of the *i*th decay component (eqn (3)) as a function of $\log(\tau_i)$. For unimodal distributions the EI method fits the lifetime's distribution to a Gaussian function and provides the mean lifetime (τ_M) and the corresponding standard deviations (σ). In the case of multi-modal distributions, the method gives the values of τ_{Mj}, σ_j and the (percentage) relative weight (RW_j) of each sub-distribution defined as:

$$RW_j = \frac{\sum_j \alpha_j \tau_j}{\sum_j \sum_i \alpha_{ji} \tau_{ji}} \quad (4)$$

From these data, the mean lifetime of the entire distribution (τ_M) can be estimated according to eqn (5):

$$\tau_M = \frac{100}{\sum_j (RW_j/\tau_{Mj})} \quad (5)$$

As expected, the τ_M calculated from the simple multiexponential fit (eqn (1)) or from the lifetime's distributions (eqn (5)) are the same within the errors introduced during the mathematical manipulation of the experimental data.

Transient absorption measurements were carried out using conventional laser-flash photolysis equipment. In brief, a Spectron SL400 Nd:YAG laser generating 355 nm laser pulses (~130 mJ per pulse, 6 ns FWHM) was used for sample excitation. The laser beam was defocused in order to cover all of the path length (10 mm) of the analyzing beam from a 150 W Xe lamp. The detection system comprises a PTI monochromator coupled to a Hamamatsu R666 PM tube. The signals were captured by a digital oscilloscope (HP54504), averaged and finally transferred to a computer for their analysis. A continuous flow cell was used in order to avoid photodecomposition of the samples by the high energy laser pulses. The stock solution used for feeding the flow cell was kept under continuous argon (or air) bubbling at (298 ± 1) K. At the excitation wavelength (355 nm), the molar absorption coefficient of A is only about 3000 M^{-1} cm^{-1}. Hence, in order to obtain reasonable excitation absorptions (~0.2–0.3), relatively concentrated NP dispersions are required (~3 mg ml^{-1}). PDA0 dispersions of this concentration can be prepared in most organic solvents. However, PAD25 and PAD75 (as well as PD25 and PD75) are not dispersible in acetonitrile at concentrations larger than ~0.2–0.3 mg ml^{-1}. As commented before, the only solvents that allow dispersing significant masses of all NPs studied are DCM and chloroform. For this reason most studies, and in particular laser flash photolysis experiments, were carried out in DCM.

3. Results and discussion

3.1 Spectroscopic characterization of PAD0, PD25 and PD75

In Fig. 1, the absorption and (corrected) emission spectra of a solution prepared by dispersing 0.8 mg ml^{-1} of PAD0 in DCM are shown. The spectra are similar to those observed for 9MA in the same solvent. The emission spectrum is independent of the excitation wavelength. Excimer formation, whose emission maximum appears around 540 nm, is not observed.[38] These results are consistent with the fact that the average number of anthracene derivatives per NP is small (~1.4). The fluorescence quantum yield of PAD0 in DCM was estimated relative to that of 9MA in *c*-hexane. Note that the measured value of ϕ_f (Table 1) is substantially larger than that shown by 9MA in fluid media. The (corrected) excitation spectrum of the PAD0 dispersion recorded at the aromatic emission maximum (~415 nm) is also shown in Fig. 1. As expected, the absorption and excitation spectra (normalized to their maxima) closely

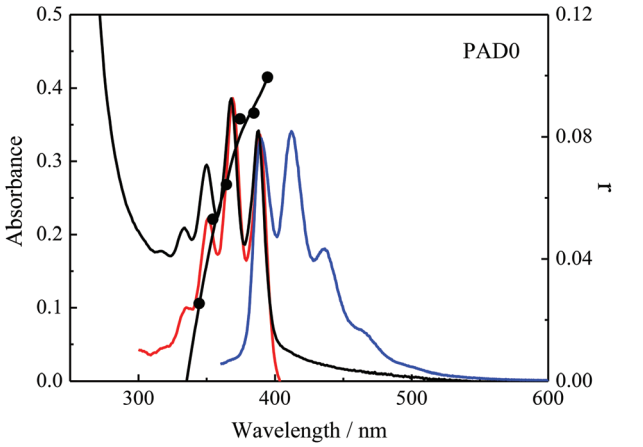

Fig. 1 Absorption (black), corrected emission (blue), corrected excitation (red) and excitation anisotropy (-●-) spectra of a dispersion of PAD0 in DCM (0.8 mg ml^{-1}) at 298 K. Excitation wavelength = 350 nm. The excitation spectrum was obtained by monitoring the emission at 415 nm. The values of the steady-state anisotropy (*r*) are shown in the right axis of the plot. Emission anisotropy was acquired with detection at 415 nm.

overlap. The excitation spectrum is independent of the emission wavelength. The black circles in Fig. 1 represent the NP steady-state excitation anisotropy spectrum. As shown, the measured fluorescence anisotropy (*r*) decreases with decreasing excitation wavelength. This behavior is typical of the anthracenyl fluorophore.[39] The observed *r* (larger than $r_0 \sim 0$ in the entire excitation wavelength range studied) strongly suggests that A is covalently linked to the polymeric matrix.

The fluorescence decay of the PAD0 dispersion after (pulsed) excitation at 378 nm is shown in Fig. 2. Fitting of the emission profile requires a bi-exponential decay function. Similar behaviors have been reported for several anthracene derivatives attached to polymeric matrices.[40,41] The parameters obtained from the fitting of the decay curves are collected in Table 3-ESI.† The result of the analysis of the emission decays according to the EI lifetime distribution method is shown in Fig. 3. The analysis indicates the existence of a bimodal distribution with maxima at ~4.0 ns and 8.6 ns, respectively. Table 1 summarizes the most important parameters obtained from this analysis. It is worth noting that all reported values of τ_{Mi}, σ_i and RW_i correspond to the average of at least four independent measurements (the standard deviation among measurements is ~10% of the reported values). As expected, the τ_M of the distribution (eqn (5)) calculated from the data in

Table 1 Photophysical characterization of the anthracenyl fluorophore (A) in different polymeric nanoparticles. All experiments were carried-out at 298 K

	Solvent	ϕ_f	τ_{M1}/ns	σ_1/ns	RW_1/%	τ_{M2}/ns	σ_2/ns	RW_2/%	τ_{M3}/ns	σ_3/ns	RW_3/%	τ_M[a]/ns
9MA	*c*-Hexane	0.35	4.6	0.01	100	—	—	—	—	—	—	4.6
	DCM	0.17	2.25	0.01	100	—	—	—	—	—	—	2.25
PAD0	DCM	0.53	4.01	0.55	21	8.6	1.8	79	—	—	—	6.93 (6.92)
PAD25	DCM	0.14	0.83	0.11	12	4.6	1.0	66	11.8	1.4	22	3.47 (3.41)
PAD75	DCM	0.04	0.78	0.16	34	3.1	0.6	55	13.4	1.0	11	1.63 (1.70)
Exciplex	DCM	—	0.97	0.20	8	4.0	0.7	29	15.2	2.5	63	—

[a] Values within parentheses correspond to the mean lifetimes obtained from the multiexponential analysis.

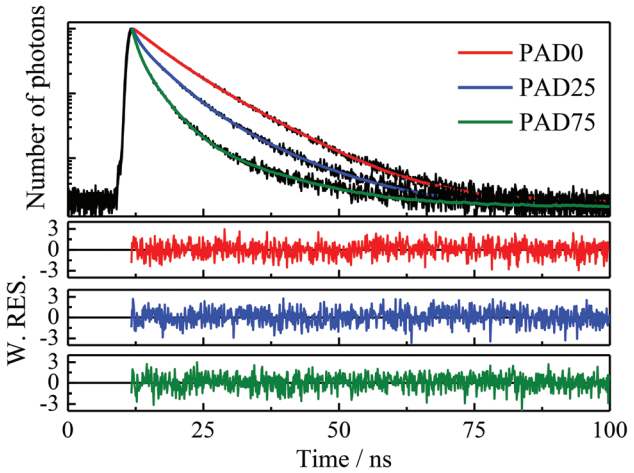

Fig. 2 TCSPC emission decay profiles (black lines) and corresponding fits (color lines) obtained for PAD0 (red), PAD25 (blue), and PAD75 dispersions (green) in DCM (298 K). Samples were not deaerated. Excitation wavelength: 378 nm. Fluorescence was collected at the emission maxima of the samples, *i.e.* ~415 nm. The calculated χ^2 were: 1.081 (PAD0), 1.011 (PAD25) and 1.116 (PAD75). Bottom panels show the corresponding color-coded residuals of the fit. The concentration of the NP dispersions was 2.5 mg ml^{-1}.

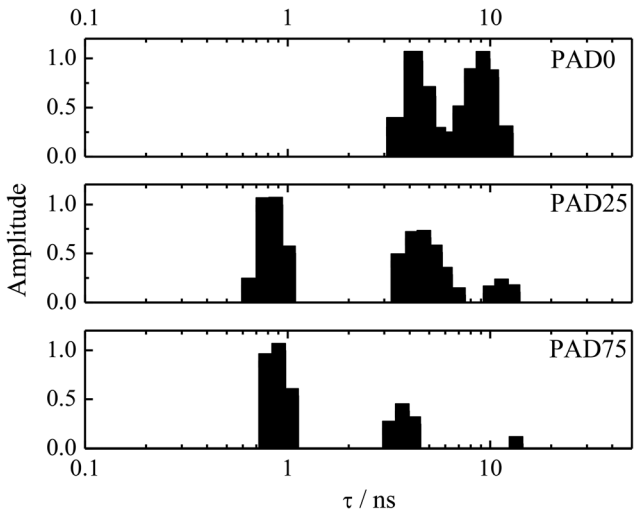

Fig. 3 Lifetime distributions as calculated for different nanoparticles in DCM (298 K). Excitation wavelength: 378 nm. Emission wavelength: 415 nm. The calculated χ^2 were: 1.080 (PAD0), 1.125 (PAD25) and 1.122 (PAD75). The concentration of the NP dispersions was 2.5 mg ml^{-1}.

Table 1 or from the fitting parameters of the bi-exponential decay (eqn (1)) (Table 3-ESI†) are nearly the same.

Results shown in Fig. 3 can be explained considering the photophysical properties of 9MA. It is known that the energy and shape (relative vibronic peak intensities) of the absorption and emission spectra of 9MA are almost insensitive to the properties of the medium. However, the τ and ϕ_f of 9MA increase markedly with increasing solvent viscosity. Blatt *et al.*[42] showed that intersystem crossing, the main non-radiative decay pathway of the singlet excited state of 9MA, is coupled to "ring-flapping" (nuclear) coordinates which can be hindered by increasing the viscosity of the solvent. In agreement with this observation, Tan *et al.*[40] found that the fluorescent lifetime of 9MA immobilized in poly(methacrylic acid) approaches the natural lifetime of its excited state (τ_0): *ca.* ~13–15 ns. Hence, results in Fig. 3 suggest that the anthracenyl fluorophore in PAD0 senses two distinct microenvironments. In both cases, the probe seems to be partially immobilized affecting the normal relaxation process of its singlet excited state. The first subsets in the lifetime distribution can be assigned to fluorophores located in relatively roomy or flexible cavities inside the polymer and the second to a group of fluorophores deeply trapped into the highly rigid crosslinked polymeric network.

The absorption and emission spectra of PD25 and PD75 are similar to those of *N*,*N*-dimethylaniline (DMA) in fluid solution. Both types of NPs are poorly fluorescent in DCM. This is apparently due to the quenching of the amine excited state by the chlorinated solvent. In *c*-hexane, DCM quenches the emission of DMA with a $k_q \sim 1.5 \times 10^8$ M^{-1} s^{-1}. Quenching of DMA fluorescence by other chloroalkanes has been previously reported.[43] In neat DCM the ϕ_f of the aromatic amine is <5% of that observed in *c*-hexane. The emission lifetime of DMA in DCM could not be determined because it is shorter than the temporal resolution of our TSPC instrument (~100 ps). Similar limitations were found for the determination of the fluorescence lifetimes of PD25 and PD75 in DCM. These results suggest that DCM penetrates deeply into the cross-linked polymer network of these small NPs. This was confirmed by studying the emissive properties of the NPs in THF. The absorption and emission spectra of PD25 and PD75 in THF are shown in Fig. 2-ESI.† As shown in Table 2, in THF, the emission efficiencies of DMA, PD25 and PD75 are similar to those observed for DMA in *c*-hexane. As shown in Fig. 3-ESI,† the excitation spectrum of a dilute PD75 (0.02 mg ml^{-1}) recorded at the emission maximum of D (~350 nm) satisfactorily agrees with the absorption spectra of the aromatic amine. The emission of D confined in the NPs is polarized. The excitation fluorescence anisotropy spectrum of the same sample is also shown in Fig. 3-ESI.† The value of *r* is relatively constant across the $S_0 \rightarrow S_1$ transition and decreases with increasing excitation energy.

The analysis of emission decay profiles according to the EI method shows bimodal lifetime distributions for both NPs, Fig. 4. The distribution obtained for PD75 in THF shows a relatively small peak (RW_1 = 8%) with τ_M (~700 ps) and a second major subensemble (RW_2 = 92%) with τ_M similar to that observed for the DMA in THF (~2.5 ns). Unfortunately, studies on the photophysics of DMA in restricted/rigid environments have not been reported, making it difficult to rationalize the observed distributions.

Interestingly, the photophysical properties of PD25 and PD75 are nearly identical. This fact suggests that intra-NP energy transfer between D* and the surrounding D acting as S–S energy acceptors is not a relevant process in these systems.

3.2 Quenching of PAD0 emission by DMA in DCM

Photoinduced electron transfer between polyaromatic compounds and aromatic amines has been studied for more

Table 2 Photophysical characterization of the aniline fluorophore (D) in different polymeric nanoparticles. All experiments were carried out at 298 K

	Solvent	ϕ_f	τ_{M1}/ns	σ_1/ns	RW_1/%	τ_{M2}/ns	σ_2/ns	RW_2/%	τ_{M3}/ns	σ_3/ns	RW_3/%	τ_M[a]/ns
DMA	*c*-Hexane	0.11	2.4	0.01	100	—	—	—	—	—	—	0.11
	THF	0.088	2.61	0.15	100	—	—	—	—	—	—	2.59
PD25	THF	0.076	0.57	0.09	7	2.25	0.59	93	—	—	—	1.89 (1.93)
PD75	THF	0.075	0.68	0.08	8	2.53	0.47	92	—	—	—	1.89 (2.10)
PAD25	THF	0.072	0.70	0.10	12	2.35	0.45	88	—	—	—	1.82 (1.84)
PAD75	THF	0.036	0.29	0.10	14	1.34	0.48	79	4.60	0.28	7	0.90 (1.09)

[a] Values within parentheses correspond to the mean lifetimes obtained from the multiexponential analysis.

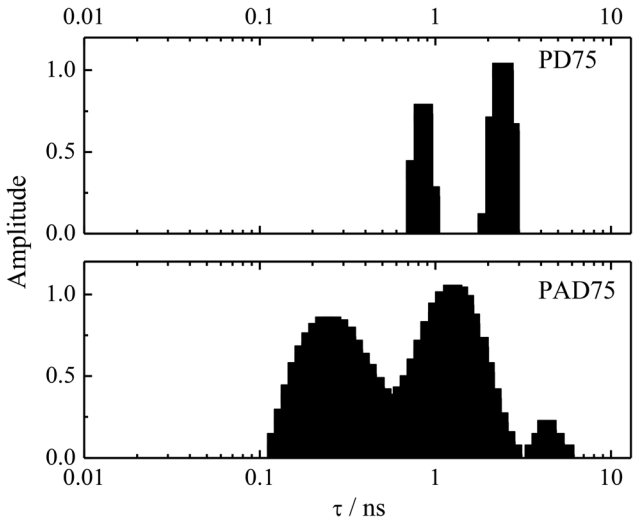

Fig. 4 Lifetime distributions as calculated for PD75 and PAD75 in THF (298 K). Excitation wavelength: 297 nm. Emission wavelength: 350 nm. The calculated χ^2 were: 1.080 (PD75) and 1.125 (PAD75). The concentration of the NP dispersions was 0.6 mg ml^{-1}.

than five decades. In particular, anthracene/aromatic amine systems have been extensively investigated in homogeneous solutions.[44–47] However, to the best of our knowledge, a comprehensive study on the intermolecular quenching of 9MA emission by DMA has not been reported. Hence, we conducted a series of experiments to better characterize this system. The results of these studies are summarized in the following paragraphs.

Quenching of the singlet excited state of 9MA by DMA approaches the diffusion rate constant limit in all solvents studied (see Table 4-ESI†). This is in agreement with the large driving force calculated for the forward photoinduced eT process (details of these calculations are given in the ESI† file). Stern–Volmer plots obtained in DCM from steady-state (I_0/I) and time resolved (τ_0/τ) emission experiments are shown in Fig. 4-ESI.† At low concentrations of DMA both plots closely match. From the initial slope of these plots ($K_{SV} \sim 26.1$ M^{-1}) a k_q value of $\sim 1.6 \times 10^{10}$ M^{-1} s^{-1} can be estimated. At larger concentrations of the amine quencher, the I_0/I plot shows an apparent upward curvature. This behavior is due to transient effects on the quenching process[32,48] that, unfortunately, cannot be studied in detail due to the limited resolution of our TCSPC instrument. Consequently, the I_0/I plot was analyzed using the sphere of action static quenching model (Perrin's model):[49]

$$\frac{I_0}{I} = \frac{\tau_0}{\tau}\exp^{(VN_A[Q])} = \left(1 + k_q\tau_0[Q]\right)\exp^{\left(\frac{4\pi N_A[Q]}{3R_{AD}^3}\right)} \quad (6)$$

where R_{AD} is the radius of the sphere of action and N_A is Avogadro's number. Details of this analysis are provided in the ESI.† The R_{AD} calculated was ~9.3 Å. Similar values of R_{AD} have been reported for the anthracene/aniline system.[50] Note that R_{AD} slightly exceeds the sum of the radii of the donor–acceptor pair (*ca.* 6.3 Å) as calculated by using Zissimos's model.[51] The emission of the 9MA–DMA exciplex can be observed in media of low to medium polarities. For instance, the emission spectrum of the exciplex in ethyl ether is shown in Fig. 5-ESI.† As expected, the emission energy of the CT state decreases as the polarity of the medium increases (see Fig. 6-ESI†). Both the 9MA and the exciplex decay mono-exponentially in all media studied suggesting that the formation of the CT state is irreversible.[52–54] The main non-radiative decay route of the CT state is the intersystem crossing to the anthracene triplet excited state. The triplet state shows a strong absorption at ~430 nm.[46,55,56]

In low to medium polarity media, the formation of the DMA cation radical ($DMA^{+\bullet}$) and anthracene anion radical ($Ant^{-\bullet}$) can be detected during exciplex lifetime (*i.e.*, on the ns time scale).[44] $DMA^{+\bullet}$ shows a broad absorption band centered at ~480 nm[44,57] and $Ant^{-\bullet}$ presents a set of peaks in the 650–750 nm wavelength region.[57,58] The low permittivity of these media prevents radical ion separation favoring the back-electron transfer process. In polar solvents, photoinduced eT leads to the formation of free radical ion pairs. In Fig. 7-ESI,† the (normalized) transient absorption spectra for 9MA and 9MA–DMA recorded 5 μs after the laser pulse in acetonitrile and DCM are compared. In the absence of the quencher, 9MA shows only the absorption corresponding to the triplet excited state of the aromatic (~430 nm). In the presence of DMA 0.4 M, the absorption due to $DMA^{+\bullet}$ and $Ant^{-\bullet}$ can be detected in acetonitrile. As expected, free radical ion formation is not observed after excitation of 9MA–DMA in DCM.

Fig. 5 shows the quenching of PAD0 emission by DMA in DCM. The corresponding Stern–Volmer plot is shown in Fig. 6. In contrast to that observed for the 9MA–DMA system, the Stern–Volmer plot shows a downward curvature. The quenching is accompanied by the appearance of an isoemissive point

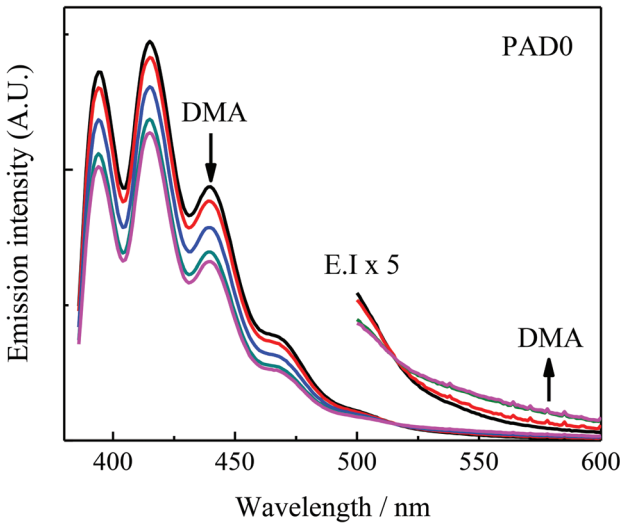

Fig. 5 Quenching of PAD0's emission by DMA: 0 M (black), 0.043 M (red), 0.093 M (blue), 0.141 M (cyan), and 0.222 M (magenta). Solvent: DCM. Excitation wavelength = 350 nm. The concentration of the NP dispersion was 1.0 mg ml^{-1}.

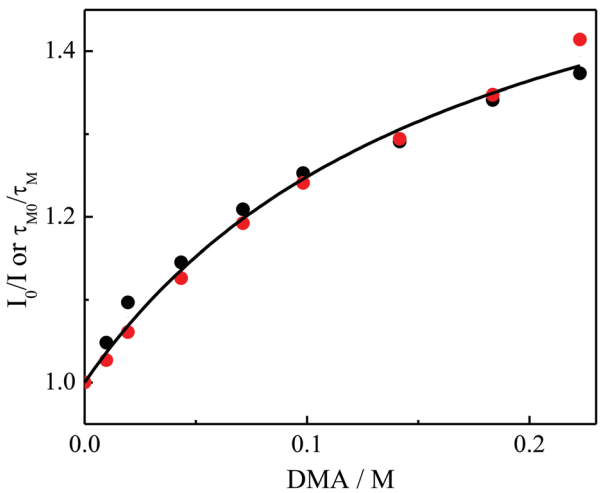

Fig. 6 Stern–Volmer plot obtained from steady state (I_0/I, red circles) and time resolved (τ_{M0}/τ_M, black circles) emission experiments. Quenching of PAD0 by DMA in DCM (298 K). The solid line represents the best fit of eqn (8) (main text) to the experimental data.

at ~515 nm and a very slight increase of the emission intensity between 500 and 600 nm. At the maximum concentration of DMA studied (0.222 M), approximately 30% of the NP emission is quenched. At the same fraction of quenching, the 9MA–DMA system (in DCM) shows a prominent emission of the intermolecular exciplex at ~530 nm. It is well known that anthracene–aromatic amine systems form "sandwich" type exciplexes.[59,60] The stabilization of these intermolecular CT states requires an appropriate distance and spatial orientation between the donor and acceptor molecules. Results shown in Fig. 5 suggest that the polymer matrix hampers exciplex formation. Hence, the photoinduced eT process appears to lead

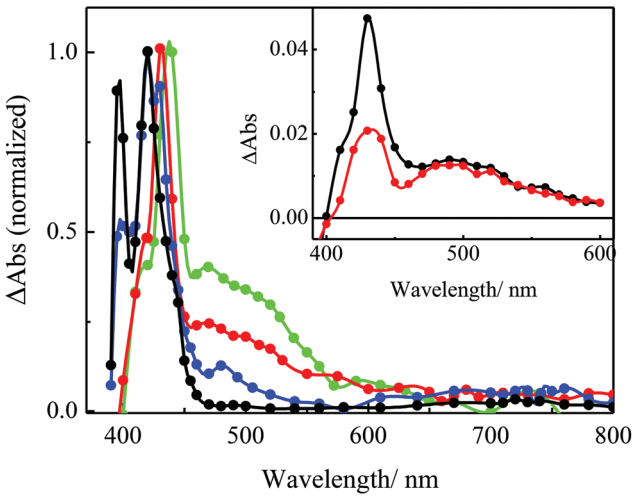

Fig. 7 Normalized transient absorption spectra obtained at 1 μs after laser excitation for dispersions of PAD0 (black), PAD0 + DMA 0.40 M (blue), PAD25 (red) and PAD75 (green). Samples were deaerated. The inset shows the transient absorption spectra obtained at 3 μs after the laser excitation pulse for dispersion of PAD25 under argon (black) and air atmosphere (red). Solvent: DCM; laser excitation at 355 nm. The concentration of the NP dispersions was 2.5 mg ml^{-1}.

to the formation of poorly interacting radical ion pairs such that the formation of the exciplex is significantly precluded.

In order to confirm the existence of a photoinduced eT process from the excited state of the anthracenyl moiety to the DMA quencher, transient absorption spectra were recorded by the laser flash photolysis technique. Experiments were carried-out in acetonitrile and DCM. Results obtained in acetonitrile are shown in Fig. 7-ESI.† As can be concluded, the system behaves similarly to the 9MA–DMA in the same media. Fig. 7 shows the transient absorption spectra of the studied NPs recorded in DCM 1 μs after the laser pulse. The band observed around 430 nm is assigned to the triplet excited state of the anthracenyl chromophore.[46] PAD0 shows an additional band around 400 nm which originates from the transient absorption A*. This (unexpected) long lived S_1 state is generated by triplet–triplet annihilation when high intensity laser pulses are used. This phenomenon was studied in detail by Saltiel *et al.*[61] The transient absorption spectrum of PAD0 in the presence of DMA 0.4 M shows a small peak around 480 nm, which can be attributed to the radical cation of DMA.[57] Further experimental evidence of this assignation, as well as the analysis of the transient absorption spectra obtained for the other NPs, are discussed in detail in section 3.3. Curiously, the formation of $Ant^{-\bullet}$ is not observed in DCM.

The analysis of the PAD0 emission decays according to the EI method at three different concentrations of the DMA is shown in Fig. 8. The data obtained for all the samples studied are shown in Table 3. As shown in Fig. 8, at a relatively low concentration of DMA (<0.05 M) the entire lifetime distribution shifts to shorter values and becomes broader. Interestingly, above DMA 0.07 M the lifetime's distribution splits into three subensembles. As the concentration of the quencher

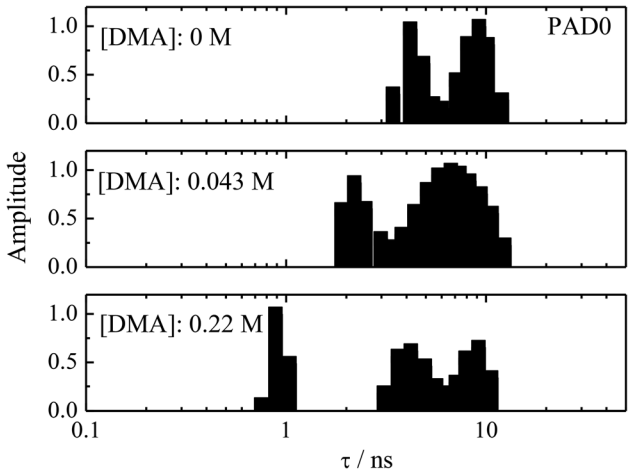

Fig. 8 EI lifetime's distribution analysis of a dispersion of PAD0 in DCM (298 K) at different concentrations of the DMA. The calculated χ^2 were 1.059, 1.140 and 0.983 for 0.000, 0.043 and 0.222 M of DMA, respectively. Excitation wavelength: 378 nm. Emission wavelength: 415 nm. The concentration of the NP dispersions was 1.0 mg ml^{-1}.

increases, the subensembles' widths (σ) progressively narrow, although their relative weights (RW) do not change significantly. Data in Table 3 were used to calculate τ_M at each concentration of DMA according to eqn (5). The plot of τ_{M0}/τ_M is shown in Fig. 6. The good agreement between the I_0/I and τ_{M0}/τ_M plots indicates that the quenching is mainly dynamic (diffusion dependent) in the entire range of [DMA] studied. The downward curvature of the Stern–Volmer plot suggests the existence of multiple fluorophore populations with different accessibilities to the quencher.

A general model for the interpretation of the emission quenching in microheterogeneous systems was proposed by Carraway *et al.*[62] The model was applied to luminescence quenching of $Ru(phen)_3^{+2}$ adsorbed on silica surfaces by oxygen. The authors assumed the existence of a finite number (k) of the fluorophore populations, each decaying monoexponentially and able to be quenched by oxygen with the same rate constant k_q. For the case of a purely dynamic quenching, it was shown that:

$$\frac{I_0}{I} = \frac{\tau_{M0}}{\tau_M} = \left[\sum_{i=1}^{k} \frac{RW_{0i}}{(1 + k_q\tau_{0i}[Q])}\right] = \sum_{i=1}^{k} RW_{0i}\tau_i \qquad (7)$$

where $RW_{0i} = \alpha_{0i}\tau_{0i}/\sum_{i=1}^{k}\alpha_{01}\tau_{0i}$ and $\tau_i = \tau_{0i}/(k_q\tau_{0i}[Q])$ represent the relative weight to the total emission and the lifetime of the ith population, respectively. The decay profile for the unquenched Ru(II) complex was fitted to a bi-Gaussian lifetime's distribution. Interestingly, these results are similar to our previously described results; that is, the adsorbed Ru(II) complex also shows two well-defined initial populations that shift to shorter times upon addition of oxygen. Assuming k_q = 1×10^6 M^{-1} s^{-1}, the emission decay profiles at different concentrations of oxygen were also fitted (resulting in bi-modal non-Gaussian distributions) and the corresponding values of τ_M were calculated. The existence of an acceptable correlation between experimental I_0/I and τ_{M0}/τ_M led Carraway *et al.*[62] to conclude that the quenching was virtually all dynamic, and more importantly, that the observed correlation could be taken as a validation of the method.

However, and besides this apparent success, Carraway's model involves several assumptions that are difficult to justify. Note that the lifetime distributions do not contain any information regarding the accessibility of the quencher to the fluorophores. Carraway *et al.* assume that the accessibility is the same since they suppose an identical k_q for all fluorophores.

As discussed in section 3.1 the lifetime's distribution observed for the A in PAD0 can be attributed to the restrictions imposed by the polymeric matrix on the normal relaxation processes of A*. In principle, it is reasonable to expect that those fluorophores showing the longest τ_{0i} are located in the most rigid microenvironments and consequently should be the most difficult to be reached by the quencher. In contrast, Carraway's model assumes that the longer lived fluorophores are more heavily quenched.

Another aspect omitted in Carraway's analysis is the impossibility to "trace" the different fluorophore populations with changing concentrations of the quencher. Note that two fluorophores showing similar τ_{0i} and contributing to the initial lifetime's distribution of amplitude α_{0i} may have different accessibility to the quencher (Q) and therefore they could be quenched with different rate constants k_{qi}. Thus, in the presence of Q these two apparently identical populations will split, and their individual amplitudes will be plotted at two different values of τ_i. This "transfer" between subensembles cannot be predicted, making the estimation of quenching

Table 3 Average lifetime (τ), standard deviations (σ) and the relative weight of each subensemble (RW) of PAD0 at different concentrations of DMA in DCM

DMA/M	τ_{M1}/ns	σ_1/ns	RW_1/%	τ_{M2}/ns	σ_2/ns	RW_2/%	τ_{M3}/ns	σ_3/ns	RW_3/%	τ_M/ns
0	4.01	0.55	18	8.62	1.89	82	—	—	—	6.94
0.0098	3.48	0.53	17	8.13	2.08	83	—	—	—	6.25
0.0195	2.86	0.39	14	7.89	1.93	86	—	—	—	6.33
0.0434	2.18	0.29	9	7.36	2.53	91	—	—	—	6.06
0.0712	1.66	0.18	7	4.76	0.84	30	9.14	1.81	63	5.74
0.0983	1.51	0.18	7	4.55	0.80	29	9.10	1.80	64	5.54
0.1417	1.25	0.12	6	4.37	0.76	29	9.08	1.76	65	5.38
0.1835	1.11	0.11	6	4.18	0.71	27	8.99	1.77	67	5.17
0.2227	1.00	0.08	5	4.51	0.75	32	9.43	1.54	63	5.06

rate constants (k_{qi}) for each component of the subensembles simply impossible.

Hence, the only realistic solution to this problem would be to obtain k_q distributions using single molecule (or single particle) fluorescence techniques. Quite interesting examples of the use of this technique for that purpose have been published recently by Lian *et al.*[63] Unfortunately, given the intrinsic nature of the systems studied herein (low fluorescence quantum yields, absorption and emission at relatively short wavelengths, apparent irreversibility of the quenching process, *etc.*) conducting this experiment seems not feasible in the near future.

In this complex context, we tried to extract some kinetic information from the Stern–Volmer plots by analyzing the experimental data according to:

$$\frac{I_0}{I} = \frac{\tau_{M0}}{\tau_M} = \left[\sum_{i=1}^{n} \frac{RW_n}{(1 + K_{SVn}[Q])}\right]^{-1} \quad (8)$$

Eqn (8) is a simplification of eqn (7) that assumes the existence of a discrete number (n) of fluorophore populations, each characterized by a particular RW_n and able to be quenched with an average Stern–Volmer constant (K_{SVn}). While it may look odd, eqn (8) is just the general Stern–Volmer expression for the quenching of n fluorophore populations with different accessibilities to the quencher. The solid line in Fig. 6 shows the best fit of eqn (8) to the experimental data with n = 2 (increasing n did not produce any apparent improvement in the quality of the fitting). The obtained values for RW_1, RW_2, K_{SV1} and K_{SV2} were: 41%, 59%, 9 M^{-1} and 0.1 M^{-1}, respectively. These results indicate that about 60% of A* cannot be reached by the quencher. Although this result seems to agree in some way with the data in Table 3 (the average lifetime of the long-lived excited state subensemble, τ_{M3}, does not change significantly with [Q] and it represents approximately 65% of the total emission), the actual lifetime's distribution indicates that the overall quenching process is much more complex.

3.3 Intra-NP PeT processes

Fig. 9 shows the absorption and emission spectra obtained for dispersions of PAD25 and PAD75 in DCM. The absorption bands centered around 305 nm are typical of the DMA chromophore. The spectra show also the characteristic absorption of the anthracene chromophore between 300 and 400 nm. The emission spectra obtained upon excitation of the polyaromatic (*ca.* 369 nm) are also shown in Fig. 9. Although the emission spectra of PAD25 and PAD75 are similar to those observed for PAD0 (Fig. 1), they show an increased emission around 500–600 nm. This effect becomes apparent when the normalized emission spectra of the NPs are compared (see Fig. 8-ESI†). In principle, this new band can be assigned to the formation of the intra-particle D–A exciplex (*vide infra*). The ϕ_f measured for the anthracenyl fluorophore (A) in PAD25 is ~0.14 (Table 1). Taking into account that the ϕ_f measured for PAD0 is 0.53, the low ϕ_f measured for PAD25 suggests a significant quenching of the polyaromatic emission (~74%) in this

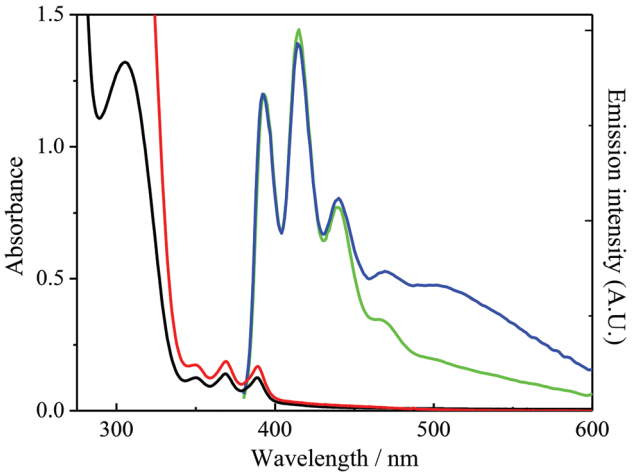

Fig. 9 Absorption spectrum obtained for PAD25 (0.6 mg ml^{-1}) (black) and PAD75 (1.36 mg ml^{-1}) (red) in DCM at 298 K. Corrected emission spectra normalized at 375 nm obtained for PAD25 (green) and PAD75 (blue) by excitation at 368 nm.

type of particle. The ϕ_f for PAD75 in DCM is ~0.04, indicating that approximately 92% of the emission of A is being quenched.

The emission decay profiles obtained for PAD0, PAD25 and PAD75 dispersions are shown in Fig. 2. Fitting of the decays required tri-exponential decay functions; and as expected, the EI analysis showed complex lifetime distributions (see Table 1 and Fig. 3). Interestingly, the percentages of quenching calculated from the τ_M for PAD25 and PAD75 (relative to the τ_M of PAD0) are ~50% and 74%, respectively. These values are much smaller than those calculated from the corresponding ϕ_f. Hence, it may be concluded that the intra-NP quenching of the anthracenyl fluorophore involves static and dynamic components. The static quenching must be a very fast process and, therefore, undetectable with our TCSPC instrument. Similar results for the ET mediated quenching of $Ru(bpy)_3^{+2*}$ by anthracene in (semirigid) poly(ethylene glycol) dimethacrylate monoliths were reported by Meyer *et al.*[64] The authors attributed the observed dynamic quenching to a slow bimolecular process which requires diffusion of the reactants in the semi-rigid polymeric medium.

The lifetime distributions obtained for PAD25 and PAD75 in DCM are shown in Fig. 3. Both distributions show a new subensemble centered at ~800 ps when compared with the lifetime distribution of PAD0. The relative weight (RW) of this new subset clearly increases with increasing concentration of the amine quencher in the NPs. Since both A and D are covalently linked to the polymeric matrices, the observed "dynamic" quenching cannot involve translation (diffusion) of the reactants. Accordingly, the lifetime distributions do not show the typical behavior observed for bimolecular quenching processes (see for example Fig. 8). Hence, these subensembles with τ_{M1} ~ 800 ps must represent also a first order quenching process. In principle, this process may be attributed to long-range eT quenching of the anthracenyl fluorophore by D. This

supposition seems to be in agreement with the gradual disappearance of the second ($\tau_{M2} \sim 4$ ns) and third ($\tau_{M3} \sim 10$ ns) subensembles with increasing [D] in the polymer matrix. Apparently, the fluorophores that are not being quenched during their excited state lifetimes sense similar microenvironments to those in PAD0 (see Fig. 3). Obviously, the existence of these "isolated" fluorophores becomes rarer with increasing concentration of the quencher in the polymeric matrices.

We used Perrin's model to estimate the A*–D critical distances (R_{AD}) for the "overall" quenching process. To this end, we used the experimental ϕ_f and τ_M (Table 1) according to:

$$\mathrm{Ln}\left(\frac{\phi_{fPAD0}}{\phi_{fPADi}}\right) = \frac{4\pi N_A}{3{R_{AD}}^3}[Q] \quad (9)$$

where i = 25 or 75 indicates the NPs studied, and [Q] is the concentration of the quencher (D) as calculated in the pre-polymeric mixtures, *ca.* 1.12 M and 2.45 M for PAD25 and PAD75, respectively. The good linear correlation observed in Fig. 9-ESI† suggests a Poisson-like distribution of amine donors around the anthracenyl fluorophore. From this plot, a value of $R_{AD} \sim 7.5$ Å was calculated. It is worth noting that this critical distance is just an average value. As mentioned above, an important fraction of the quenching is undetectable for our TCSPC setup. The fast quenching component probably occurs at very small A*–D separation distances, close to contact. Therefore, the slow component represented by the subensemble with $\tau_M \sim 800$ ps should be a photoinduced eT process taking place at $R > 7.5$ Å.

As shown in Fig. 8-ESI,† the emission maximum of the intra-NP exciplex is observed around 510–520 nm. To estimate the polarity of the microenvironment sensed by this exciplex a Lippert–Mataga plot for the intermolecular 9MA–DMA exciplex was constructed (see Fig. 6-ESI†). The results indicate that the intra-NP exciplex is sensing an intermediate polarity between ethyl acetate and ethyl ether, which is in agreement with the composition of the polymers. Further information about formation/deactivation processes of the intra-NP exciplex was obtained from time-resolved fluorescence experiments. Within the time resolution of our TCSPC instrument, the formation of the exciplex appears to be instantaneous. Fig. 10-ESI† shows the time resolved emission spectrum (TRES) obtained for PAD75 in DCM in the 450–600 wavelength range. At shorter times, the spectrum is dominated by the emission of the anthracenyl fluorophore which extends beyond 550 nm. As the emission of the polyaromatic disappears, the characteristic spectrum of the exciplex becomes apparent. Table 1 shows the results of the EI lifetime's distribution analysis of the exciplex's emission collected at 520 nm. The distribution is trimodal. The two first subsets centered at ~1 and ~4 ns, respectively, can be associated with the decay of the singlet excited state of A (see Fig. 3). The last subset ($\tau_M \sim 15$ ns) represents the decay of the intra-NP exciplex. This lifetime of the intra-NP exciplex is similar to that observed for the intermolecular 9MA/DMA exciplex in fluid media (Table 4-ESI†).

The (normalized) transient absorption spectra for PAD25 and PAD75 in DCM, recorded 1 μs after a laser excitation pulse under an argon atmosphere, are displayed in Fig. 7. The spectra show the characteristic absorptions of the triplet excited state of the anthracenyl residue (~430 nm) and that of $D^{+\bullet}$ (~480 nm). The triplet excited state of DMA absorbs in the same range of wavelengths as $D^{+\bullet}$. However, these two species can be easily distinguished by their reactivity towards oxygen. The inset in Fig. 7 shows the transient spectra of PAD25 under an inert (argon) atmosphere and in the presence of air. As expected, the absorption band attributed to the triplet state of A is quenched. In contrast, the absorption at ~480 nm does not change, indicating that this band does not have a significant contribution from the triplet excited state of D. Thus, the detection of $D^{+\bullet}$ can be taken as clear evidence of intra-NP PeT taking place in these systems. However, formation of the radical anion of the polyaromatic is observed in none of the NPs studied. Hence, $A^{-\bullet}$ must react with impurities present in the polymeric matrices. It has been shown that $Ant^{-\bullet}$ reacts quickly with a vast number of substrates (including traces of water in the solvent),[58] an experimental fact that supports our hypothesis.

The relatively increased absorption observed at 480 nm for PAD75 (compared to that of PAD25) can be attributed to the larger percentage of intra-NP quenching of A* in these NPs, which causes an increase in the transient concentration of $D^{+\bullet}$ at the expense of triplets' population. Finally, it is important to note that the lifetime of $D^{+\bullet}$ (recorded at 500 nm) shows a similar trend for all the systems studied (experiments not shown). After a fast initial decrease, the transient absorption reaches a plateau that persists on the ms time scale. This behavior can be rationalized considering the lack of a reducing agent in the medium after depletion of $A^{-\bullet}$.

3.4 Intra-NP ET processes

The absorption and emission spectra of a dilute dispersion of PAD25 (0.8 mg ml^{-1}) in THF obtained by preferential excitation to the amine chromophore (at 306 nm) are shown as a green continuous line in Fig. 10. The fluorescence peak detected around 350 nm corresponds to that of D. Interestingly, the spectrum shows also the emission of A. Note that this emission cannot arise from a direct excitation of the polyaromatic since at that particular wavelength (306 nm) the fraction of light absorbed by A is negligible compared to that of the aromatic amine.

In Fig. 11, the excitation spectrum of the dispersion obtained by recording the emission at 415 nm (the emission maximum of the anthracenyl chromophore) is shown. In the same figure, the excitation steady-state anisotropy (r) spectrum was plotted. The excitation spectrum has contributions from both the A and D chromophores. These results can be taken as evidence for the singlet–singlet ET process from D* to A. The excitation anisotropy spectrum shows high values of r for the anthracene absorption band (as observed for PAD0), but r is negligibly small for those wavelengths corresponding to the absorption of D. Both results are consistent with the singlet–

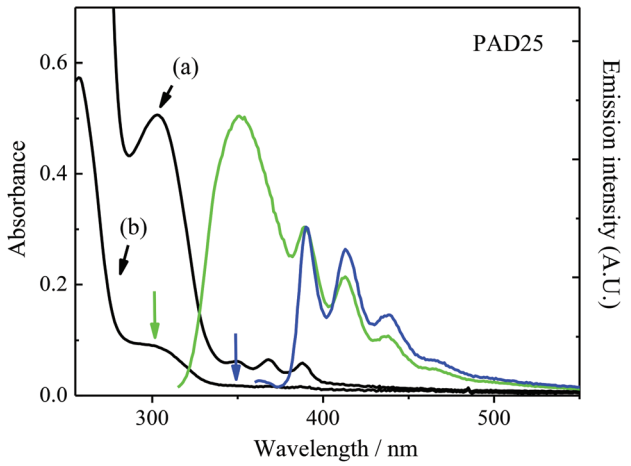

Fig. 10 (a) Absorption spectrum of a dispersion of PAD25 (0.8 mg ml^{-1}) in THF and (b) absorption spectrum of a dispersion of PAD25 (0.15 mg ml^{-1}) in the same solvent. Emission spectra obtained by excitation of the dispersions at 368 nm (blue) and 306 nm (green). Arrows indicate the corresponding excitation wavelengths.

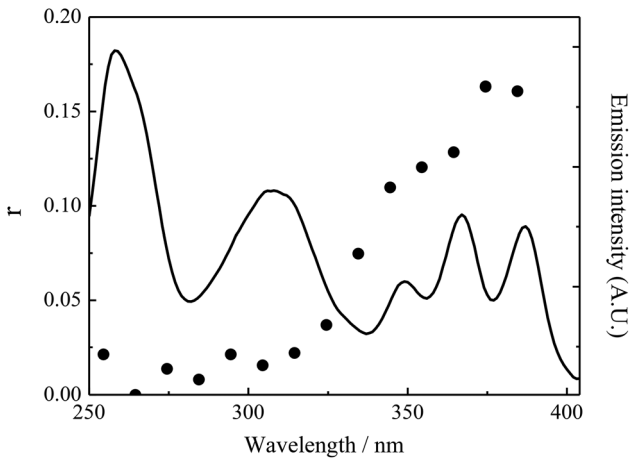

Fig. 11 Excitation spectrum of a diluted dispersion of PAD25 (0.15 mg ml^{-1}) in THF. Emission wavelength: 440 nm. The excitation steady-state anisotropy (r) spectrum is represented by the solid black circles; emission was also collected at 440 nm. The actual values of r are shown in the left axis of the plot.

singlet Föster resonance ET mechanism. Energy transfer taking place from D* to randomly oriented A chromophores should lead to complete depolarization of the polyaromatic emission. Experiments carried-out for PAD75 in THF show analogous results (Fig. 11-ESI and 12-ESI†).

The reported E_{00} for D and A are 429 and 316 kJ mol^{-1},[59] respectively, making $\Delta E_{00} \sim -113$ kJ mol^{-1}. The critical distance (R_0) for the Föster resonance ET process was calculated from the overlap of the emission spectrum of DMA and the absorption spectrum of 9MA (assuming an orientation factor $\kappa^2 = 2/3$). The obtained value was ~2.7 nm. Thus, the D to A Föster ET process should be fairly favorable in these small NP systems ($d < 9$ nm). Although in principle Dexter ET is also possible, this mechanism requires very short separation distances between the D–A pair (close contact) and under such circumstances direct formation of the radical ion pair should occur precluding ET.

In principle, an estimation of the intra-NP efficiencies for ET (Φ_{ET}) can be accomplished by comparing the experimental ϕ_f (or τ_M) measured for PD25, PD75, PAD25 and PAD75. As shown in Table 2, the ϕ_f and τ_M estimated for PAD25 are slightly smaller than those of PD25. However, the values for PAD75 and PD75 differ significantly. In Fig. 4, the lifetime distributions of these two last mentioned NP types are compared. It is apparent that the distribution for PAD75 shifts to shorter lifetimes and becomes much broader as compared to the lifetime distribution of PD75, suggesting a highly heterogeneous ET process. The lifetime distribution also shows a small third subensemble at ~4 ns. It is worth noting that given the low ϕ_f observed for PAD75 at 350 nm, relatively broad emission slits were used to obtain reliable decay profiles in reasonable acquisition times. Hence, the third subset can be attributed to spurious light arising from the sensitized emission of A.

From the experimental data in Table 2, approximate values of Φ_{ET} were calculated according to:

$$\Phi_{ET} = 1 - \frac{\phi_f^{PDi}}{\phi_f^{PADi}} = 1 - \frac{\tau_M^{PDi}}{\tau_M^{PADi}} \quad (10)$$

where i = 25 or 75 refers to the different NPs studied. Thus, average values of ~0.04 (±0.01) and ~0.50 (±0.06) were obtained for PAD25 and PAD75, respectively. In turn, these values can be used to calculate the average D*–A separation distance (R). The values of R obtained were ~5.0 (±0.5) and ~2.7 (±0.2) nm for PAD25 and PAD75, respectively. As expected, this calculated R reveals the much closer D*–A pair average separation in PAD75.

4. Conclusions

Five types of NPs dispersible in organic media were synthesized and characterized. The method used for the preparation of these NPs can be adapted to the synthesis of MIP NPs, opening an exciting prospect for the synthesis of new materials with multiple applications.

Although the kinetics of the inter- and intra-PeT (and ET) processes occurring in these NPs are always complex, some interesting conclusions can be drawn from these studies. As expected both types of processes (PeT and ET) can be used for the optical detection of an analyte. In principle, the fluorophores attached to the NPs (A or D) can be taken as the transducer, while the quencher emulates the analyte. It was shown that the solvent (DMC) is able to penetrate all NPs. However, results obtained from the quenching of PAD0 by DMA indicate that important diffusional barriers are imposed by the polymeric matrix on the quencher. An actual MIP NP should have an improved permeability, which may probably be achieved by decreasing the amount of cross-linker or including a porogen during the preparation of the NPs.

Glossary

A	9-Methylanthracene-acrylate derivative (9-anthracenylmethyl methacrylate) incorporated into the polymeric nanoparticles
α_i	The corresponding amplitude of the *i*th component of the multiexponential decay
D	*N*,*N*-Dimethylaniline-acrylate derivative (*N*-(4-dimethylamino-benzyl)-2-methyl-acrylamide) incorporated into the polymeric nanoparticles
DCM	Dichloromethane
DLS	Dynamic light scattering
EGDMA	Ethylene glycol dimethacrylate
EI method	The lifetime's distribution analysis software provided by Edinburgh Instruments
eT	Electron transfer process
ET	Energy transfer process
k_q	Quenching rate constant
K_{SV}	Stern–Volmer rate constant
9-MA	9-Methylanthracene
MMA	Methyl methacrylate
NPs	Nanoparticles
PAD0	NP composed of a crosslinked polymer matrix of methyl methacrylate, ethylene glycol dimethacrylate and a low doping level of A
PAD25	NP composed of a crosslinked polymer matrix of methyl methacrylate, ethylene glycol dimethacrylate, D and a low doping level of A. 25% of the mole fraction of methyl methacrylate (relative to PAD0) is replaced by D
PAD75	NP composed of a crosslinked polymer matrix of methyl methacrylate and ethylene glycol dimethacrylate, D and a low doping level of A. 75% of the mole fraction of methyl methacrylate (relative to PAD0) is replaced by D
PD25	NP composed of a crosslinked polymer matrix of methyl methacrylate, ethylene glycol dimethacrylate and D. 25% of the mole fraction of methyl methacrylate (relative to PAD0) is replaced by D
PD75	NP composed of a crosslinked polymer matrix of methyl methacrylate, ethylene glycol dimethacrylate and D. 75% of the mole fraction of methyl methacrylate (relative to PAD0) is replaced by D
PeT	Photoinduced electron transfer process
r	Excitation steady-state anisotropy spectrum
R_0	Critical distance for the Föster resonance ET process
R_{AD}	Radius of the sphere of action (Perrin's model)
RW	Relative weight
TCSPC instrument	Time-correlated single-photon counting fluorometer
THF	Tetrahydrofuran
TRES	Time resolved emission spectrum
V	Volume of the sphere of action (Perrin's model)
α_i	Opulation of fluorophores characterized by an emission lifetime τ_i in the continuous distribution of the lifetime model assumed by the EI method
τ	Fluorescence lifetime
τ_M	Mean fluorescence lifetime
Φ_{ET}	Efficiency for energy transfer
ϕ_f	Fluorescence quantum yield
σ	Standard deviation of a Gaussian distribution

Acknowledgements

The authors thank the Consejo Nacional de Investigaciones Científicas y Técnicas (CONICET-Argentina), Agencia Nacional de Promoción Científica (FONCYT-Argentina) and Secretaría de Ciencia y Técnica (UNRC) for financial support. C. S. thanks CONICET for a PhD scholarship. J.J.T. and N.G. thank CONICET-MinCyT (Córdoba) for PhD scholarships.

References

1 *Molecularly imprinted materials: science and technology*, ed. M. Yan and O. Ramström, CRC press, New York, 2005.
2 Á. Valero-Navarro, M. Gómez-Romero, J. F. Fernández-Sánchez, P. A. G. Cormack, A. Segura-Carretero and A. Fernández-Gutiérrez, Synthesis of caffeic acid molecularly imprinted polymer microspheres and high-performance liquid chromatography evaluation of their sorption properties, *J. Chromatogr., A*, 2011, **1218**, 7289–7296.
3 M. C. Moreno-Bondi, F. Navarro-Villoslada, E. Benito-Pena and J. L. Urraca, Molecularly Imprinted Polymers as Selective Recognition Elements in Optical Sensing, *Curr. Anal. Chem.*, 2008, **4**, 316–340.
4 D. Cunliffe, A. Kirby and C. Alexander, Molecularly imprinted drug delivery systems, *Adv. Drug Delivery Rev.*, 2005, **57**, 1836–1853.
5 S. Gao, W. Wang and B. Wang, Molecularly Imprinted Materials as Recognition Elements in Optical Sensors, in *Molecularly Imprinted Materials. Science and Technology*, ed. M. Yan and O. Ramstrom, M. Dekker, New York, 2005.
6 H. Kim and G. Guiochon, Thermodynamic Studies of the Solvent Effects in Chromatography on Molecularly Imprinted Polymers. 3. Nature of the Organic Mobile Phase, *Anal. Chem.*, 2005, **77**, 2496–2504.
7 B. Wandelt, P. Turkewitsch, S. Wysocki and G. D. Darling, Fluorescent molecularly imprinted polymer studied by time-resolved fluorescence spectroscopy, *Polymer*, 2002, **43**, 2777–2785.
8 C. Lindstrom and X. Zhu, Photoinduced electron transfer at molecule-metal interfaces, *Chem. Rev.*, 2006, **106**, 4281–4300.
9 B. O'Regan and M. Gratzel, A low-cost, high-efficiency solar cell based on dye-sensitized, *Nature*, 1991, **353**, 737–740.

10 M. Grätzel, Photoelectrochemical cells, *Nature*, 2001, **414**, 338–344.
11 U. Bach, D. Lupo, P. Comte, J. Moser, F. Weissörtel, J. Salbeck, H. Spreitzer and M. Grätzel, Solid-state dye-sensitized mesoporous TiO_2 solar cells with high photon-to-electron conversion efficiencies, *Nature*, 1998, **395**, 583–585.
12 J. B. Asbury, E. Hao, Y. Wang, H. N. Ghosh and T. Lian, Ultrafast Electron Transfer Dynamics from Molecular Adsorbates to Semiconductor Nanocrystalline Thin Films, *J. Phys. Chem. B*, 2001, **105**, 4545–4557.
13 A. P. Kulkarni, C. J. Tonzola, A. Babel and S. A. Jenekhe, Electron Transport Materials for Organic Light-Emitting Diodes, *Chem. Mater.*, 2004, **16**, 4556–4573.
14 P.-T. Chou and Y. Chi, Phosphorescent Dyes for Organic Light-Emitting Diodes, *Chem.–Eur. J.*, 2007, **13**, 380–395.
15 M. C. Gather, A. Köhnen and K. Meerholz, White Organic Light-Emitting Diodes, *Adv. Mater.*, 2011, **23**, 233–248.
16 J. Mabeck and G. Malliaras, Chemical and biological sensors based on organic thin-film transistors, *Anal. Bioanal. Chem.*, 2006, **384**, 343–353.
17 C. D. Dimitrakopoulos and P. R. Malenfant, Organic thin film transistors for large area electronics, *Adv. Mater.*, 2002, **14**, 99–117.
18 H. Sirringhaus, Device Physics of Solution-Processed Organic Field-Effect Transistors, *Adv. Mater.*, 2005, **17**, 2411–2425.
19 J. Zaumseil and H. Sirringhaus, Electron and ambipolar transport in organic field-effect transistors, *Chem. Rev.*, 2007, **107**, 1296–1323.
20 J. C. Scott and L. D. Bozano, Nonvolatile Memory Elements Based on Organic Materials, *Adv. Mater.*, 2007, **19**, 1452–1463.
21 B. Liu and G. C. Bazan, Optimization of the Molecular Orbital Energies of Conjugated Polymers for Optical Amplification of Fluorescent Sensors, *J. Am. Chem. Soc.*, 2006, **128**, 1188–1196.
22 J. Kong, N. R. Franklin, C. Zhou, M. G. Chapline, S. Peng, K. Cho and H. Dai, Nanotube Molecular Wires as Chemical Sensors, *Science*, 2000, **287**, 622–625.
23 P. J. S. Gomes, C. Serpa, R. M. D. Nunes, L. G. Arnaut and S. o. J. Formosinho, Exothermic Rate Restrictions in Long-Range Photoinduced Charge Separations in Rigid Media, *J. Phys. Chem. A*, 2010, **114**, 2778–2787.
24 O. S. Wenger, B. S. Leigh, R. M. Villahermosa, H. B. Gray and J. R. Winkler, Electron Tunneling Through Organic Molecules in Frozen Glasses, *Science*, 2005, **307**, 99–102.
25 M. A. Fox, Introduction - Electron Transfer: A Critical Link between Subdisciplines in Chemistry, *Chem. Rev.*, 1992, **92**, 365–368.
26 A. Ponce, H. B. Gray and J. R. Winkler, Electron Tunneling through Water: Oxidative Quenching of Electronically Excited Ru(tpy)22+ (tpy = 2,2′:6,2″-terpyridine) by Ferric Ions in Aqueous Glasses at 77 K, *J. Am. Chem. Soc.*, 2000, **122**, 8187–8191.
27 T. Guarr, M. E. McGuire and G. McLendon, Long range photoinduced electron transfer in a rigid polymer, *J. Am. Chem. Soc.*, 1985, **107**, 5104–5111.
28 H. Ohkita and S. Ito, Transient absorption spectroscopy of polymer-based thin-film solar cells, *Polymer*, 2011, **52**, 4397–4417.
29 S. S. Atik and J. K. Thomas, Photoinduced electron transfer in organized assemblies, *J. Am. Chem. Soc.*, 1981, **103**, 3550–3555.
30 S. S. Atik and J. K. Thomas, Photochemistry in polymerized microemulsion systems, *J. Am. Chem. Soc.*, 1982, **104**, 5868–5874.
31 I. B. Berlman, *Handbook of Fluorescence Spectra of Aromatic Molecules*, ACS Publications, New York and London, 2nd edn, 1971.
32 J. R. Lakowicz, *Principles of fluorescence spectroscopy*, Springer, New York, 3rd edn, 2006.
33 B. Valeur, *Molecular fluorescence: principles and applications*, Wiley-VCH, Weinheim, 2002.
34 A. Siemiarczuk, B. D. Wagner and W. R. Ware, Comparison of the maximum entropy and exponential series methods for the recovery of distributions of lifetimes from fluorescence lifetime data, *J. Phys. Chem.*, 1990, **94**, 1661–1666.
35 M. A. El-Kemary and I. M. El-Mehasseb, Global and distribution analysis of fluorescence decays and spectrofluorimetric determination of stoichiometry and association constant of the inclusion complex of 2-amino-5,6-dimethylbenzimidazole with β-cyclodextrin, *Talanta*, 2004, **62**, 317–322.
36 *Operating-Instructions*, Edinburgh Analytical Instruments, Riccarton, Currie, Edinburgh, UK, EHI4 4AP, 1995.
37 J. Malicka, R. Ganzynkowicz, M. Groth, C. Czaplewski, J. Karolczak, A. Liwo and W. Wiczk, Fluorescence decay time distribution analysis of cyclic enkephalin analogues; Influence of solvent and Leu configuration in position 5 on conformation, *Acta Biochim. Pol.*, 2001, **48**, 95–102.
38 J. K. McVey, D. M. Shold and N. C. Yang, Direct observation and characterization of anthracene excimer in solution, *J. Chem. Phys.*, 1976, **65**, 3375–3376.
39 C. Wang, J. Xu and R. G. Weiss, Factors Influencing Orientations of Covalently-Attached and Doped Aromatic Groups in Stretched Polyethylene Films, *J. Phys. Chem. B*, 2003, **107**, 7015–7025.
40 K. L. Tan and F. E. Treloar, Solubilization of 9-methylanthracene by the hypercoiled form of poly(methacrylic acid) in water: fluorescence decay and rotational diffusion measurements, *Chem. Phys. Lett.*, 1980, **73**, 234–239.
41 M. J. Tiera and M. G. Neumann, Anthracene-Bound Fluorescence Studies of Methacrylic Acid-co-Methylmethacrylate Copolymers, *J. Braz. Chem. Soc.*, 1995, **6**, 191–197.
42 E. Blatt, F. E. Treloar, K. P. Ghiggino and R. G. Gilbert, Viscosity and temperature dependence of fluorescence lifetimes of anthracene and 9-methylanthracene, *J. Phys. Chem.*, 1981, **85**, 2810–2816.

43 M. F. Budyka and M. V. Alfimov, Photochemical reactions of complexes of aromatic amines with polyhalomethanes, *Russ. Chem. Rev.*, 1995, **64**, 705.
44 M. Mac, J. Najbar and J. Wirz, Fluorescence quenching of derivatives of anthracene by organic electron donors and acceptors in acetonitrile. Electron and proton transfer mechanism, *Chem. Phys. Lett.*, 1995, **235**, 187–194.
45 G. J. Kavarnos and N. J. Turro, Photosensitization by reversible electron transfer: theories, experimental evidence, and examples, *Chem. Rev.*, 1986, **86**, 401–449.
46 M. Ottolenghi, C. R. Goldschmidt and R. Potashnik, Intersystem crossing in the charge-transfer quenching of molecular fluorescence, *J. Phys. Chem.*, 1971, **75**, 1025–1031.
47 H. Beens, H. Knibbe and A. Weller, Dipolar Nature of Molecular Complexes Formed in the Excited State, *J. Chem. Phys.*, 1967, **47**, 1183–1184.
48 J. Keizer, Nonlinear fluorescence quenching and the origin of positive curvature in Stern-Volmer plots, *J. Am. Chem. Soc.*, 1983, **105**, 1494–1498.
49 F. Perrin, *C. R. Hebd. Seances Acad. Sci.*, 1924, **178**, 1978–1980.
50 A. Reddy, J. Thipperudrappa, D. Biradar, M. Lagare and S. Hanagodimath, Fluorescence quenching of anthracene by aniline in different solvents, *Indian J. Pure Appl. Phys.*, 2004, **42**, 648–652.
51 Y. H. Zhao, M. H. Abraham and A. M. Zissimos, Fast Calculation of van der Waals Volume as a Sum of Atomic and Bond Contributions and Its Application to Drug Compounds, *J. Org. Chem.*, 2003, **68**, 7368–7373.
52 W. R. Ware, D. Watt and J. D. Holmes, Exciple photophysics. I. The α-Cyanonaphthalene-Olefin System, *J. Am. Chem. Soc.*, 1974, **96**, 7853–7860.
53 J. B. Birks, D. J. Dyson and I. H. Munro, 'Excimer' Fluorescence. II. Lifetime Studies of Pyrene Solutions, *Proc. R. Soc. London, Ser. A*, 1963, **275**, 575–588.
54 M. S. Altamirano, M. del Valle Bohorquez, C. M. Previtali and C. A. Chesta, Proton-Transfer Mediated Quenching of Pyrene/Indole Charge-Transfer States in Isooctane Solutions, *J. Phys. Chem. A*, 2008, **112**, 589–593.
55 M. Ottolenghi, Charge-transfer complexes in the excited state. Laser photolysis studies, *Acc. Chem. Res.*, 1973, **6**, 153–160.
56 G. P. Zanini and H. A. Montejano, Solvent Effects in the Electron Transfer Quenching of the Triplet State of Anthracene by p-Benzoquinones, *Bol. Soc. Chil. Quím.*, 2001, **46**, 81–90.
57 T. Shida, *Electronic absorption spectra of radical ions*, Elsevier Amsterdam, 1988.
58 S. U. Pedersen, T. Bo Christensen, T. Thomasen and K. Daasbjerg, New methods for the accurate determination of extinction and diffusion coefficients of aromatic and heteroaromatic radical anions in N,N-dimethylformamide, *J. Electroanal. Chem.*, 1998, **454**, 123–143.
59 N. Beens and A. Weller, Excited molecular π-complexes in solution, in *Organic molecular photophysics*, ed. J. Birks, Wiley and Sons, New York, 1975, pp. 159–215.
60 M. Lee and M. Lee, Structure and Solvent Dependence of the Exciplex Formation and Dissociation of Anthracene/*N*,*N*-Dimethylaniline Derivatives in n-Alkane Solvents, *Bull. Korean Chem. Soc.*, 1997, **18**, 1054–1055.
61 J. C. del Valle, A. M. Turek, N. D. Tarkalanov and J. Saltiel, Distortion of the Fluorescence Spectrum of Anthracene with Increasing Laser Pulse Excitation Energy, *J. Phys. Chem. A*, 2002, **106**, 5101–5104.
62 E. R. Carraway, J. N. Demas and B. A. DeGraff, Luminescence quenching mechanism for microheterogeneous systems, *Anal. Chem.*, 1991, **63**, 332–336.
63 N. Song, H. Zhu, S. Jin, W. Zhan and T. Lian, Poisson-Distributed Electron-Transfer Dynamics from Single Quantum Dots to C60 Molecules, *ACS Nano*, 2010, **5**, 613–621.
64 A. Ito, D. J. Stewart, Z. Fang, M. K. M. K. Brennaman and T. J. Meyer, Sensitization of ultra-long-range excited-state electron transfer by energy transfer in a polymerized film, *Proc. Natl. Acad. Sci. U. S. A.*, 2012, **109**, 15132–15135.